analytical chemistry

pubs.acs.org/ac Article

Disaggregation Behavior of Amyloid β Fibrils by Anthocyanins Studied by Total-Internal-Reflection-Fluorescence Microscopy Coupled with a Wireless Quartz-Crystal Microbalance Biosensor

Kentaro Noi, Kensuke Ikenaka, Hideki Mochizuki, Yuji Goto, and Hirotsugu Ogi*

Cite This: *Anal. Chem.* 2021, 93, 11176–11183 Read Online

ACCESS | Metrics & More | Article Recommendations | Supporting Information

ABSTRACT: Amyloid fibrils are formed from various proteins, some of which cause the corresponding neurodegenerative disorders, such as Alzheimer's and Parkinson's diseases. It has been reported that many compounds inhibit the formation of amyloid fibrils. Anthocyanins are flavonoid pigments present in fruits and vegetables, which are known to suppress symptoms related with Alzheimer's disease. However, the influence of anthocyanins on the amyloid fibril remains unclear. Here, we succeeded in the direct monitoring of the disaggregation reaction of single amyloid β (Aβ) fibrils by anthocyanins using total-internal-reflection-fluorescence microscopy with a quartz-crystal microbalance (TIRFM-QCM). It is found that the disassembly activity to the Aβ fibrils depends on the number of hydroxyl groups in six-membered ring B of anthocyanin, and only delphinidin-3-galactoside, possessing three hydroxyl groups there, shows high disassembly activity. Our results show the importance of the number of hydroxyl groups and demonstrate the usefulness of TIRFM-QCM as a powerful tool in studying interactions between amyloid fibrils and compounds.

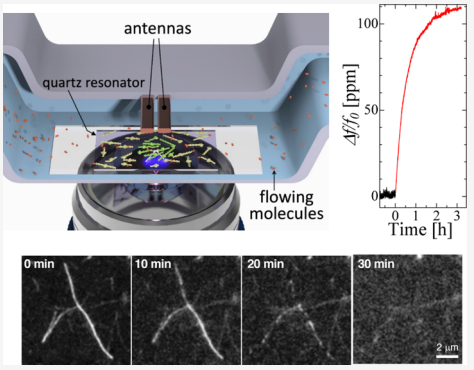

INTRODUCTION

Aggregates of amyloidogenic proteins often cause neurodegenerative disorders.[1] For example, amyloid β (Aβ) peptide and α-synuclein are causative factors for Alzheimer's disease (AD) and Parkinson's disease (PD), respectively. A common feature of the amyloidogenic proteins is that they undergo conformational change from monomeric native to highly ordered β-sheet-rich amyloid fibrils.[1,2] Oligomeric aggregates generated during the amyloid fibril formation are thought to be associated with the neurotoxicity and thus the development of neurodegenerative diseases.[3−5] There are, therefore, many reports on compounds and proteins, which inhibit and/or disassemble the amyloid fibrils. Representative natural compounds are (−)-epigallocatechine-3-gallate (EGCG),[6−11] which is a type of catechin, curcumin,[12−14] and pyrroloquinoline quinone (PQQ).[15,16] It is also reported that proteins such as molecular chaperones[17−19] and cyclophilins[20] suppress the amyloid fibril formation. Thus, research studies for finding new compounds and molecules for inhibition and disassembly against amyloid fibrils and clarification of their mechanisms remain a central issue.

Recently, it is found that anthocyanins can be promising candidates for inhibiting the fibril formation and suppressing the neurotoxicity of amyloid fibrils.[21−23] This finding is considerably important because they are flavonoid pigments which induce red, blue, and purple colors in fruits and vegetables, and we can easily ingest them ordinarily. Their inhibitory effects on AD have been indicated *in vivo*[23,24] and in cells[25] as well as their beneficial effects on health such as antioxidant activity.[26−28] The inhibitory ability has been evaluated macroscopically through the thioflavin-T (ThT) fluorescence assay, where the ThT fluorescence level was monitored during the aggregation reactions of amyloidogenic proteins. However, considering the fact that some compounds inhibit the binding ability of ThT molecules to the amyloid fibrils, the macroscopic ThT assay would be inappropriate for evaluating the inhibitory and dissolving abilities of anthocyanins.[29−31] Therefore, in order to understand the effects of anthocyanins on the amyloid fibrils accurately and deeply, it is needed to directly detect the dynamics of the interaction between them on a single fibril, which has never been achieved because of measurement difficulties.

The total-internal-reflection-fluorescence-microscopy (TIRFM) observation was performed to study the fibril elongation behavior[32,33] in a microscopic scale, but it is inadequate to discuss the disassembly ability of anthocyanin because disappearance of a fibril would also be caused by

Received: April 22, 2021
Accepted: July 26, 2021
Published: August 5, 2021

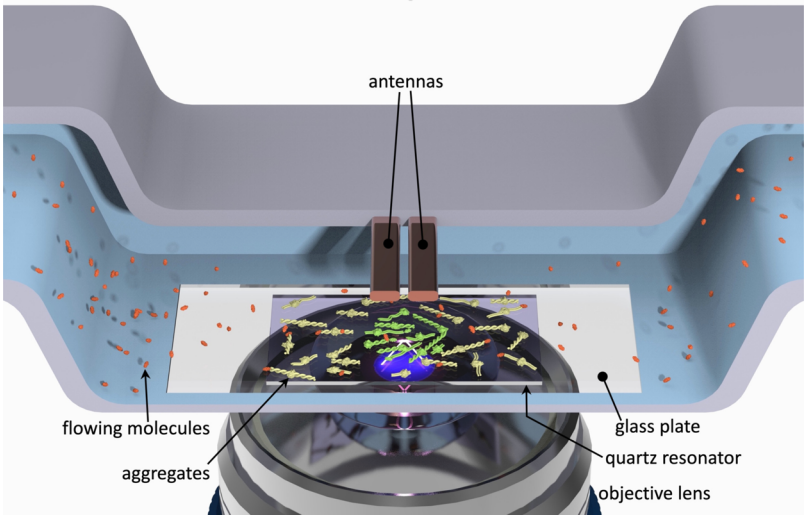

Figure 1. Schematic of the TIERFM-QCM measurement system. The antennas for generation and detection of the shear vibration of the quartz resonator are embedded inside the flow-cell upper wall (the half part of the upper wall is removed in this figure to show details inside the flow cell).

desorption of ThT molecules from the fibril or by their degradation of the emission ability due to excess light absorption, not only by the disaggregation of the fibril. Here, we use the wireless−electrodeless quartz-crystal microbalance (WE-QCM) biosensor combined with TIRFM for dynamically studying the interactions between anthocyanins and amyloid β (Aβ) fibrils in a microscopic region. We call this original technique TIRFM-QCM. The QCM biosensor is a mass-sensitive label-free biosensor, which allows detection of mass change on the quartz crystal oscillator surface through the change in the resonance frequency.[34,35] Because electrodes and wires needed to excite the quartz resonator significantly deteriorate the mass sensitivity of the QCM biosensor,[36] WE-QCM has been originally developed.[37,38] It significantly improves the mass sensitivity, and more importantly, the electrodeless aspect allows a microscopic observation on the sensor surface during the biosensor measurement owing to the transparent quartz crystal. WE-QCM has been thus incorporated in a TIRFM system.[39,40] This TIRFM-QCM measurement allows simultaneous observation of the fibril structure change and the mass change on the sensor surface during the solution flow. Therefore, we can accurately evaluate the disaggregation behavior of fibrils through both the mass change detected using the QCM biosensor and the structure change observed by TIRFM.

There are various types of anthocyanins according to the type and number of sugars and the number and position of hydroxy and methoxyl groups on the basic anthocyanidin skeleton.[41] In this study, we focus on three galactosides [delphinidin-3-galactoside (D3-gal), cyanidine-3-galactoside (C3-gal), and malvidin-3-galactoside (M3-gal)] among them because of three reasons: (i) they tend to accumulate in tissues, especially in the cerebellum,[42] so that they may directly affect neurodegenerative diseases. (ii) It is suggested that D3-gal and C3-gal show inhibitor ability to the formation of amyloid fibrils.[21] (iii) Their concentrations are relatively larger in berries,[42] which can be ingested orally. We investigate their disassembly capability against Aβ amyloid fibrils as well as that of chlorogenic acid (CGA) as a control polyphenol using the originally developed TIRFM-QCM system, paying attention to the difference in the number of hydroxyl groups in six-membered ring B. The conventional macroscopic ThT assay is also performed to compare with the TIRFM-QCM measurements.

EXPERIMENTAL SECTION

Materials. Lyophilized-powder Aβ_{1-40} peptide and Aβ_{1-42} peptide were purchased from Peptide Institute. Dimethyl sulfoxide (DMSO), phosphate buffer solution (PBS), NaCl, and ThT were purchased from Wako Pure Chemical Industries Ltd.

Preparation of Aβ_{1-42} Seeds and Monomeric Aβ_{1-40} Solution. The lyophilized powder of Aβ_{1-42} was dissolved by DMSO and diluted to a concentration of 50 μM by an acetate buffer (ABS) with pH 4.6 containing 100 mM NaCl. The volume fraction of DMSO and the ABS solution was 1:4. This solution was stirred at 1200 rpm for 24 h to grow the seeds. The seed solution was sonicated for 1 min using a 200 kHz high-power ultrasonic generator (KAIJO, 4021). The sonicated Aβ_{1-42} seed solution was diluted by ultrapure water to 10 μM, which was used for immobilizing the Aβ_{1-42} seeds on the quartz resonator.

Lyophilized-powder Aβ_{1-40} was dissolved by DMSO and diluted to a concentration of 10 μM by ultrapure water. The volume fraction of DMSO and ultrapure water was 1:19.

ThT Fluorescence Assay. The sample solution, which contained 10 μM Aβ_{1-40} peptide, 0.5 μM Aβ_{1-42} seed, and 30 μM ThT, was dispensed into 12 wells in a 96-well microplate, and it was set in a microplate reader. Their fluorescence intensities at 485 nm were measured with a 450 nm excitation every 10 min after 50 s shaking agitation. After the ThT fluorescence intensities rose sufficiently, indicating the amyloid fibril formation, all solutions from the 12 wells were mixed together in a microbute, and the solution was dispensed into another 96-well microplate. The anthocyanin or CGA was then added to each well to a final concentration of 100 μM, and the ThT fluorescence assay was performed to evaluate its disassembly capability.

TIRFM-QCM Measurement. The TIRFM-QCM system was originally developed in our laboratory.[39] A blank AT-cut quartz-crystal resonator with a thickness of 26 μm and an area of 1.7 × 2.5 mm^2 was cleaned using a UV−ozone cleaner after

https://doi.org/10.1021/acs.analchem.1c01720
Anal. Chem. 2021, 93, 11176−11183

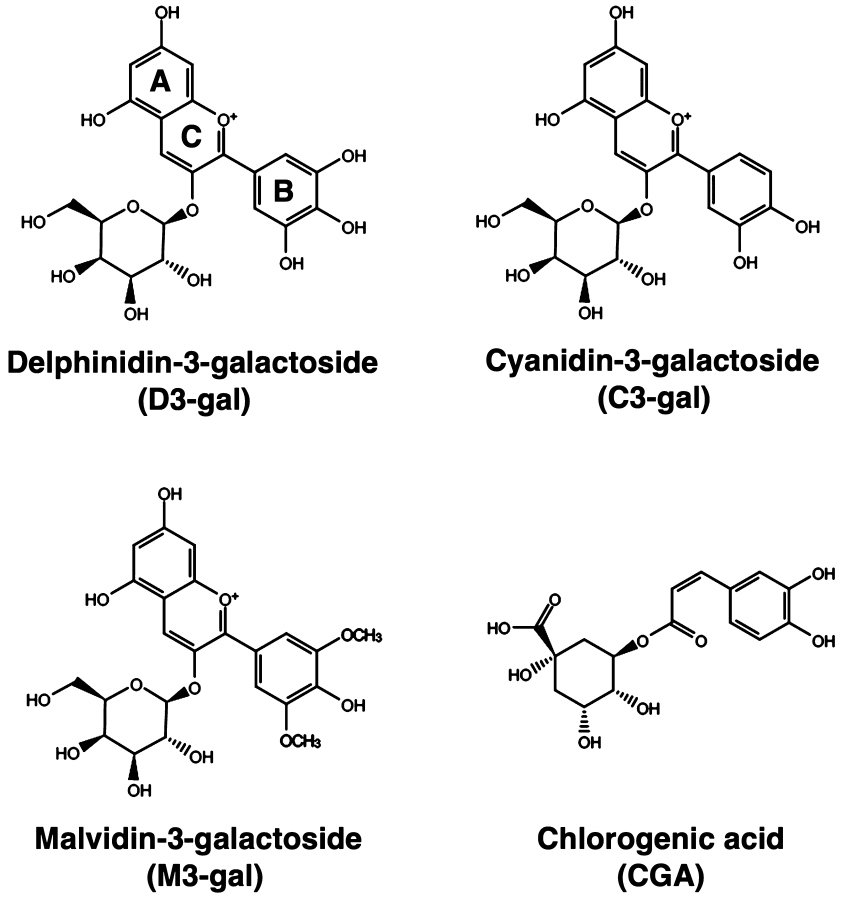

Figure 2. Chemical structures of anthocyanins and polyphenol used in this study.

washing for 15 min in a piranha solution (98% H_2SO_4/33% H_2O_2 = 7:3) and rinsing with ultrapure water. The cleaned quartz resonator was set in the sensor cell as shown in Figure 1. The 10 μM Aβ_{1-42}-seed solution was injected in the sensor cell, which was left for 24 h at 4 °C to immobilize the Aβ_{1-42} seeds on the quartz resonator. After washing the quartz resonator with ultrapure water, the 10 μM monomeric Aβ_{1-40} solution containing 30 μM ThT (pH 7.4) was flowed for ∼10 h to form the dense amyloid fibrils on the quartz resonator. After the amyloid fibril formation, the quartz resonator was washed to remove the unreacted Aβ_{1-40} by injecting the 30 μM ThT buffer solution, and the 100 μM anthocyanin or chlorogenic-acid solution containing 30 μM ThT (pH 7.4) was flowed to the sensor cell with conducting the TIRFM-QCM measurements, during which the resonance-frequency change and the TIRFM images were obtained. All TIRFM-QCM measurements were performed at a flow rate of 500 μL/min and room temperature.

Analysis of QCM Data. The amount of Aβ peptides in a unit area on the quartz resonator, σ, is calculated from the fractional change in the resonant frequency $\Delta f/f$ of the quartz resonator using the Sauerbrey equation[43]

$$\sigma = -\frac{\Delta f}{f}\frac{d_q \rho_q}{M_w} \quad (1)$$

Here, d_q and ρ_q are the thickness and mass density of the quartz resonator, respectively, and M_w denotes the molecular mass.

RESULTS

Macroscopic ThT Assay. We prepared D3-gal, C3-gal, and M3-gal as anthocyanins and CGA as a polyphenol for comparison. The principal difference among these three anthocyanins is the number of hydroxyl groups in six-membered ring B (Figure 2). First, we evaluated their disassembly capability using the macroscopic (conventional) ThT fluorescence assay. The Aβ amyloid fibrils were formed by adding Aβ_{1-40} peptides to the Aβ_{1-42} seeds inside the wells as shown in Figure S1. Figure 3 shows time courses of the ThT fluorescence intensity after adding the anthocyanins and CGA.

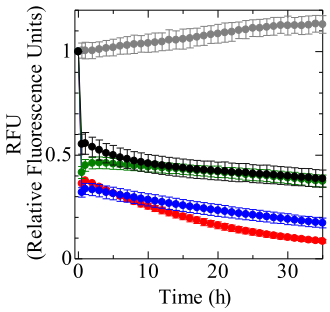

Figure 3. ThT fluorescence intensity measurement of Aβ amyloid fibrils with anthocyanins and CGA. Normalization was performed based on the fluorescence intensity at the start of the measurement, and its relative change was monitored. Gray, red, blue, green, and black marks correspond to additions of PBS, D3-gal, C3-gal, M3-gal, and CGA, respectively.

https://doi.org/10.1021/acs.analchem.1c01720
Anal. Chem. 2021, 93, 11176−11183

The fluorescence intensity drops immediately after the addition of the polyphenols, which is, however, not observed when PBS is added as a control, indicating that the first drop is caused by either the interaction between injected molecules and ThT molecules or the shield effect for the ThT emission by the injected molecules. The subsequent gradual decrease in the ThT fluorescence intensity, which is also not observed in the addition of PBS, may be interpreted by the disaggregation of the fibrils by the anthocyanins and CGA. However, some compounds have been reported to inhibit the interaction between amyloid fibrils and ThT,[29−31] and the gradual decrease of the ThT level could be caused by the detachment of the ThT molecules from the fibrils and not by the fibril disaggregation. Therefore, it is difficult to correctly evaluate their disassembly activity on the amyloid fibrils with such an indirect detecting method.

TIRFM-QCM Measurement for Aβ Amyloid Fibril Formation. To directly investigate the disassembly activity of the anthocyanins against Aβ amyloid fibrils, Aβ amyloid fibrils were formed on the quartz resonator surface in the TIRFM-QCM system. Previous studies found that a dense $A\beta_{1-40}$ fibril network can be fabricated around the $A\beta_{1-42}$ seeds immobilized on the surface,[39,44] and we adopted this method: the $A\beta_{1-42}$ seeds prepared in advance were immobilized on the resonator surface, and the $A\beta_{1-40}$ solution was flowed in a circulating manner. Figure 4a shows the time course of the amount of deposited $A\beta_{1-40}$ peptide on the quartz resonator measured by WE-QCM, which indicates that the $A\beta_{1-40}$ peptides are captured by the $A\beta_{1-42}$ seeds significantly for the first 30 min, and the deposition proceeds with a lower deposition rate. This trend is similar to that observed in the previous study, where the first adsorption reflects the formation of an amorphous structure of $A\beta_{1-40}$ peptide, and the subsequent adsorption indicates the nucleus formation and fibril elongation.[39] After the flow of the $A\beta_{1-40}$ solution, we actually observed dense fibril structures on the surface as shown in Figure 4b.

Disassembly Activity of D3-gal against Amyloid Fibrils. After the formation of the Aβ amyloid fibrils, the D3-gal solution was flowed in the TIRFM-QCM sensor cell. Figure 4a shows the change in the amount of the $A\beta_{1-40}$ peptide on the quartz resonator monitored by QCM (red line). The result indicates that $A\beta_{1-40}$ peptides in the fibrils are dissociated within ∼3 h. The surface mass becomes lower than that before the injection of the $A\beta_{1-40}$ solution, which is attributed to dissociation of initially immobilized seeds as well. Figure 4c shows the TIRFM image on the same area as Figure 4b after the flow of the D3-gal solution, where few aggregates are observable. Movie S1 shows the corresponding disassembly behavior. The same measurements were performed several times, and we observed similar dissociation behavior by D3-gal.

The TIRFM measurement dynamically reveals the decomposition behavior of the Aβ fibrils. Some fibrils are decomposed from their ends as shown in Movie S2, but most are decomposed from their side surfaces as shown in Figures 4d and S2, and in their corresponding movies (Movies S3 and S4, respectively). Figure 5a illustrates changes in the fibril length during the flow of the D3-gal solution for 70 fibrils. Decomposition begins after a lag time from the injection of the anthocyanin and is then completed within ∼2 h. The lag time varies from 10 to ∼100 min, and it poorly correlates with the initial fibril length as shown in the upper figure in Figure 5e. On the other hand, the decomposition rate, which was

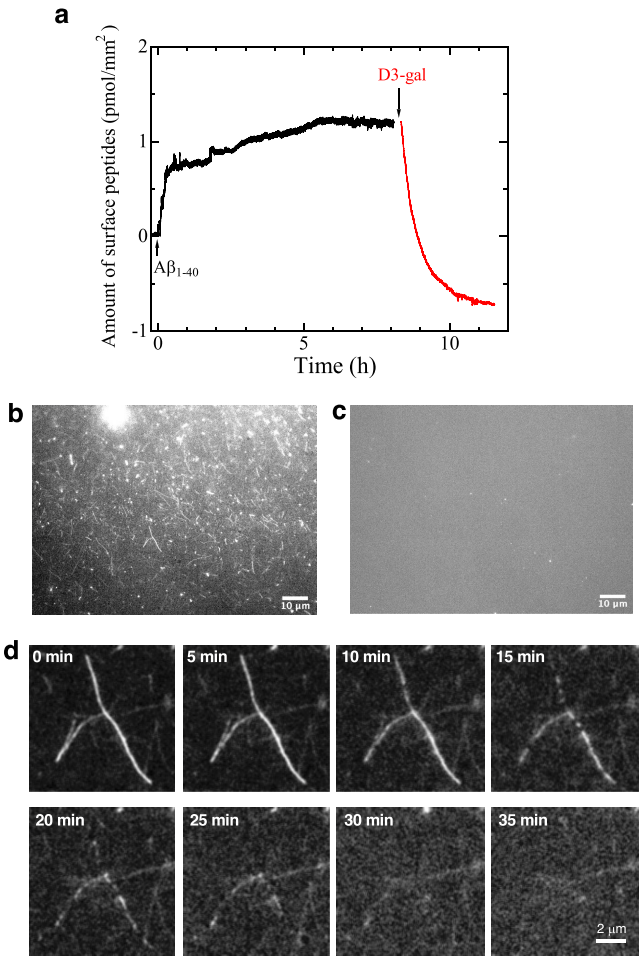

Figure 4. Aβ amyloid fibril formation and their disaggregation behavior monitored by the TIRFM-QCM system. (a) Amount of accumulated $A\beta_{1-40}$ peptide on the resonator surface during the flow of the $A\beta_{1-40}$ solution (black), and the decrease of the surface mass caused by the disassembly activity of D3-gal (red) measured by QCM. The baseline change at the injection of the D3-gal solution is corrected. (b) Fibril structure before injecting the D3-gal solution and (c) that after the flow of the D3-gal solution. (d) Disaggregation behavior of Aβ amyloid fibrils caused by D3-gal observed by TIRFM.

individually calculated from the slope in Figure 5a, shows stronger correlation with the initial fibril length. This can be consistently explained by the view that the anthocyanin molecule adsorbs onto a binding site on the fibril side wall, at which the decomposition reaction proceeds. Because the number of binding sites will be proportional to the fibril length, the decomposition rate accordingly increases for a longer fibril. The TIRFM images support this view, where the fibril decomposition proceeds from various points on the fibril side wall.

Furthermore, we observed the quartz resonator surface after the TIRFM-QCM measurements using AFM, but we could not find any fibrils or large aggregates as shown in Figure S3. Therefore, the anthocyanin D3-gal is capable of completely disassembling Aβ amyloid fibrils within a few hours.

TIRFM-QCM Measurements during Flow of Other Anthocyanins. Figure 6a−c shows time courses of the amount of $A\beta_{1-40}$ peptide on the surface measured by QCM after injections of C3-gal, M3-gal, and CGA solutions, respectively. In all measurements, we failed to observe the

https://doi.org/10.1021/acs.analchem.1c01720
Anal. Chem. 2021, 93, 11176−11183

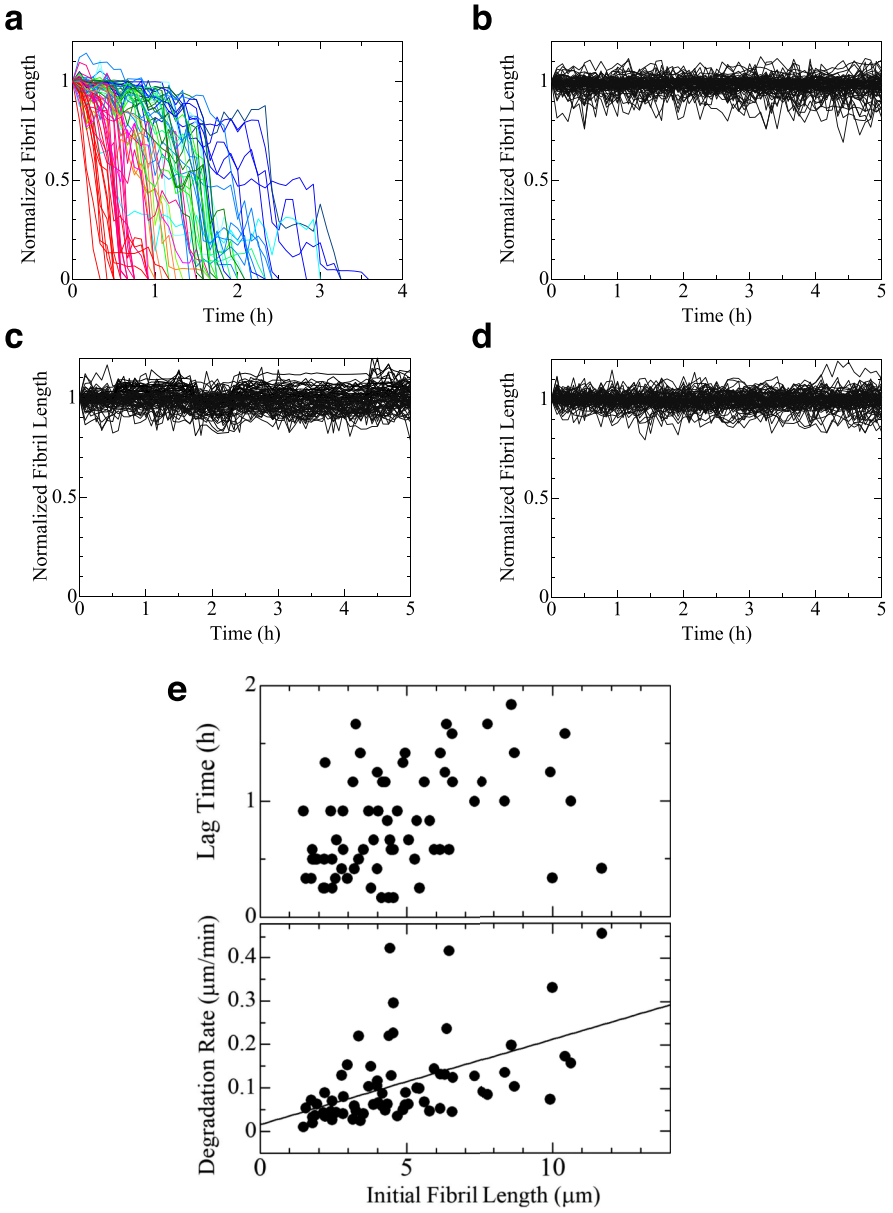

Figure 5. Disaggregation behavior of individual fibrils by (a) D3-gal, (b) C3-gal, (c) M3-gal, and (d) CGA. (e) Relationships between initial fibril length and the lag time (upper) and the decomposition rate (lower) during the flow of the D3-gal solution.

decrease in the mass on the surface unlike the measurement of D3-gal (red line in Figure 4a). Injections of M3-gal and CGA molecules caused negligible frequency changes (Figure 6b,c), demonstrating their weak interaction with Aβ_{1-40} fibrils, whereas injection of C3-gal molecules increased the surface mass (Figure 6a). This indicates that C3-gal can interact with Aβ amyloid fibrils with binding sites different from those of ThT molecules, and they are captured on the surface via the fibrils.

The TIRFM observation during flows of C3-gal, M3-gal, and CGA solutions reveals that they affect little the Aβ amyloid fibrils (Figures 5b−d and S4 and Movie S5). Therefore, C3-gal can interact with Aβ amyloid fibrils, but it does not show the disassembly activity against the fibrils. M3-gal and CGA hardly interact with the Aβ amyloid fibrils and then fail to disassemble them. These observations are significantly different from the results of the conventional (macroscopic) ThT fluorescence assay in Figure 3, where all anthocyanins appear to show the disassembly ability. Comparison of the TIRFM-QCM measurement and the ThT fluorescence assay leads an important insight that anthocyanins and CGA interfere with the interaction between Aβ amyloid fibrils and ThT molecules, indicating that the macroscopic ThT assay is inappropriate for evaluation of the disassembly activity of a candidate.

DISCUSSION

We first emphasize the importance of the TIRFM-QCM measurement. The ThT fluorescence assay has been widely used to detect amyloid fibrils. Some compounds, however, inhibit the binding of ThT to amyloid fibrils because their binding sites overlap or are close to that of ThT.[30,31] Thus, the ThT fluorescence assay would be unsuitable in evaluating the disassembly ability for such compounds. The circular dichroism (CD) spectrum measurement has also been a key method to evaluate higher-order structures of proteins. It focuses on the β-sheet structure, a characteristic structure in an

https://doi.org/10.1021/acs.analchem.1c01720
Anal. Chem. 2021, 93, 11176−11183

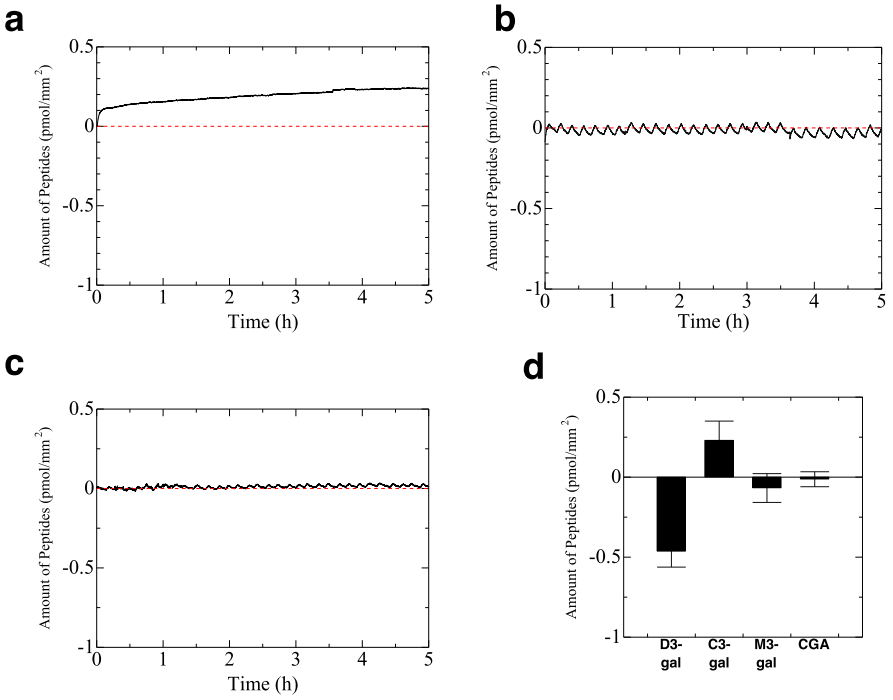

Figure 6. Change of surface mass during the flow of (a) C3-gal, (b) M3-gal, and (c) CGA solutions measured by QCM. (d) Comparison of the surface-mass change among flows of the four compounds.

amyloid fibril. It is, however, difficult to use the CD spectrum measurement for compounds and solvents, which absorb light, such as anthocyanins and DMSO, which is often used to dissolve various compounds. There are reports using SDS-PAGE and size exclusion chromatography as methods for directly detecting sizes of amyloid fibrils and oligomers.[6,11,45] However, they fail to monitor the size of aggregates in a short-time reaction in real time because it is necessary to take a sample each time. On the other hand, QCM can measure the mass change on the quartz resonator in real time, regardless of the ThT binding ability and the solvent absorbance so that we can unambiguously evaluate the dissolution dynamics precisely. At the same time, we can observe the dissolution dynamics for individual fibrils through TIRFM. This advantage allows us to identify the disassembly ability of D3-gal and binding ability of C3-gal to amyloid fibrils (Figures 4a and 6a). Only with the TIRFM observation, it would be very difficult to correctly evaluate the disassembly ability because disappearance of a fibril could also be caused by detachment of ThT molecules due to replacement with anthocyanins or failure of the β-sheet structure and not by separation of Aβ molecules from the surface after dissociation. One may attribute disappearance of fibrils during the D3-gal-solution flow to the color deterioration of ThT because of the light irradiation. However, fibrils are clearly seen even for several hours in C3-gal, M3-gal, and CGA solutions (Figure S4 and Movie S5), denying this possibility.

Next, we discuss the effect of hydroxyl groups. D3-gal and C3-gal can interact with Aβ amyloid fibrils, and D3-gal has the disassembly activity as well. M3-gal, however, fails to even interact with Aβ amyloid fibrils (Figure 6b). The most important difference among the three anthocyanins is the number of hydroxyl groups in six-membered ring B (Figure 1), suggesting that it should greatly contribute to the disassembly activity of anthocyanin. Although there are few reports investigating the effects of hydroxyl groups on galactoside, some reports appear on glucosides. Anthocyanin with glucose possessing a larger number of hydroxyl groups in six-membered ring B exhibits higher binding activity with human serum albumin (HSA).[46] Delphinidin-3-glucoside (D3-glu) and cyanidine-3-glucoside (C3-glu) will affect the stability of the second structure of HSA[46] and maintain the activity of complex I in dysfunctional mitochondria[47,48] and bind programmed cell death protein I and programmed death-ligand 1 in cancer cells.[49] Myricetin, quercetin, and kaempferol are flavonoids and possess three, two, and one hydroxyl groups in six-membered ring B, respectively. Also, the number of hydroxyl groups greatly contributed to binding ability to bovine serum albumin,[50] inhibition of Aβ and α-synuclein amyloid fibril formation,[51−53] and inhibition of curli-dependent biofilm formation.[54] EGCG, a representative catechin, is reported to inhibit amyloid fibrillogenesis and amyloid fibril disassembly and suppress cellular toxicity.[6−11] In the case of EGCG, the number of hydroxyl groups in six-membered ring B also affects the inhibition ability for Aβ_{1-42} amyloid fibrillogenesis and Aβ_{1-42} amyloid fibril disassembly[55] and binging affinity to HSA.[56,57] Thus, in many flavonoids including anthocyanin and catechin, the number of hydroxyl groups in six-membered ring B has a great influence on their binding abilities and functions. Concerning galactose-type anthocyanins, this study reveals the importance of the number of hydroxyl groups in six-membered ring B in the deterioration ability to amyloid fibrils for the first time.

Third, we discuss the lag time for disassembling fibrils. Some reports study interactions between Aβ fibrils and anthocyanins. For example, the six-membered ring B of C3-glu preferably binds to the aromatic residue Tyr10 of Aβ_{1-40} via $\pi-\pi$ interactions,[22] which could be a part of the biding site of a ThT molecule, which is captured by the shallow groove formed by continuous Tyr side chains.[58] Therefore, the binding sites of D3-gal may partially overlap with those of ThT, and for fibrils on which the binding sites of D3-gal have been already

https://doi.org/10.1021/acs.analchem.1c01720
Anal. Chem. 2021, 93, 11176−11183

occupied by ThT molecules, a longer time is required for a D3-gal molecule to bind to the fibril side. The lag time for dissociating fibrils by D3-gal will then depend on the number of remaining D3-gal's binding site on the fibril.

Finally, we discuss the effect of the detachment of ThT molecules on the TIRFM-QCM analysis. The QCM response would involve the mass unloading due to the detachment of ThT as well as that due to the disaggregation of the fibrils. However, we consider that this effect is insignificant because of two reasons. First, the detachment of ThT, if any, occurs very slowly (Figure 3) compared with the disaggregation of Aβ fibrils. Second, the molecular mass of ThT (∼319) is considerably smaller than that of the Aβ monomer (∼4300), causing less contribution to the QCM response.

CONCLUSIONS

The ThT fluorescence assay is a key methodology for detecting amyloid fibrils, but it is occasionally inappropriate in the presence of compounds. This happens in evaluating the disaggregation behavior of fibrils by light-absorbent compounds. We originally developed the TIRFM-QCM system as a powerful tool for accurately evaluating the disassembly ability of amyloid fibrils by any compounds.

We assessed the disassembly activities of three anthocyanins and CGA as a polyphenol control against Aβ amyloid fibrils using TIRFM-QCM and reveal that D3-gal shows surprisingly high disassembly ability; it completely dissolves Aβ amyloid fibrils within ∼3 h. Although C3-gal interacts with Aβ amyloid fibrils, it fails to show the disassembly activity on the fibrils. On the other hands, M3-gal and CGA cannot even bind the fibrils. We focused on the number of hydroxyl groups in six-membered ring B of the three anthocyanins. C3-gal and D3-gal have two and three hydroxyl groups, and they interact with Aβ amyloid fibrils, whereas M3-gal has only one hydroxyl group and fails to interact with the fibrils. D3-gal shows high disassembly activity to Aβ amyloid fibrils. Therefore, it is indicated that the number of hydroxyl groups in six-membered ring B, which is a characteristic structure of some flavonoids including anthocyanin, is the key parameter for the disassembly activity.

The fibrils are principally dissociated from their side walls and not from their ends. A lag time is observed in the dissociation reaction, which varies between 10 min and 2 h. We attribute this to the partial overlap in the binding sites between D3-gal and ThT: a longer time is required to dissolve a fibril, on which ThT molecules obscure the binding sites of D3-gal because of replacement of ThT with D3-gal.

ASSOCIATED CONTENT

Supporting Information

The Supporting Information is available free of charge at https://pubs.acs.org/doi/10.1021/acs.analchem.1c01720.

ThT assay during fibril formation, snapshots of TIRFM images during disaggregation behavior, and AFM images (PDF)

Movie S1: Disaggregation of many Aβ fibrils caused by D3G (AVI)

Movie S2: Disaggregation of the Aβ fibrils from edges caused by D3G (AVI)

Movie S3: Disaggregation of the Aβ fibril from a side caused by D3G (AVI)

Movie S4: Disaggregation of another Aβ fibril from a side caused by D3G (AVI)

Movie S5: Undecomposed Aβ fibrils with CGA (AVI)

AUTHOR INFORMATION

Corresponding Author

Hirotsugu Ogi − *Graduate School of Engineering, Osaka University, Suita, Osaka 565-0871, Japan;* orcid.org/0000-0001-9684-4715; Phone: +81-6-6879-7276; Email: ogi@prec.eng.osaka-u.ac.jp; Fax: +81-6-6879-7276

Authors

Kentaro Noi − *Graduate School of Engineering, Osaka University, Suita, Osaka 565-0871, Japan;* Present Address: Institute for NanoScience Design, Osaka University, Toyonaka, Osaka 560-8531, Japan

Kensuke Ikenaka − *Department of Neurology, Osaka University Graduate School of Medicine, Suita, Osaka 565-0871, Japan*

Hideki Mochizuki − *Department of Neurology, Osaka University Graduate School of Medicine, Suita, Osaka 565-0871, Japan*

Yuji Goto − *Global Center for Medical Engineering and Informatics, Osaka University, Suita, Osaka 565-0871, Japan;* orcid.org/0000-0003-1221-1270

Complete contact information is available at: https://pubs.acs.org/10.1021/acs.analchem.1c01720

Author Contributions

K.N. performed the TIRFM-QCM measurements and ThT assay and wrote the paper. K.I., H.M., and Y.G. contributed discussion on the measurements. H.O. promoted this study, developed the TIRFM-QCM system, analyzed the results, and wrote the paper.

Notes

The authors declare no competing financial interest.

ABBREVIATIONS

Aβ	amyloid β
ThT	thioflavin-T
TIRFM-QCM	total-internal-reflection-fluorescence microscopy with a quartz-crystal microbalance
AD	Alzheimer's disease
PD	Parkinson's disease
EGCG	(−)-epigallocatechine-3-gallate
PQQ	pyrroloquinoline quinone
WE-QCM	wireless−electrodeless quartz-crystal microbalance
D3-gal	delphinidin-3-galactoside
C3-gal	cyanidine- 3-galactoside
M3-gal	malvidin-3-galactoside
CGA	chlorogenic acid
D3-glu	delphinidin-3-glucoside
C3-glu	cyanidine-3-glucoside

REFERENCES

(1) Chiti, F.; Dobson, C. M. *Annu. Rev. Biochem.* **2017**, *86*, 27−68.
(2) Eisenberg, D.; Jucker, M. *Cell* **2012**, *148*, 1188−1203.
(3) Hardy, J.; Higgins, G. *Science* **1992**, *256*, 184−185.
(4) Berthelot, K.; Cullin, C.; Lecomte, S. *Biochimie* **2013**, *95*, 12−19.
(5) Hoshi, M.; Sato, M.; Matsumoto, S.; Noguchi, A.; Yasutake, K.; Yoshida, N.; Sato, K. *Proc. Natl. Acad. Sci. U. S. A.* **2003**, *100*, 6370−6375.

(6) Ehrnhoefer, D. E.; Bieschke, J.; Boeddrich, A.; Herbst, M.; Masino, L.; Lurz, R.; Engemann, S.; Pastore, A.; Wanker, E. E. *Nat. Struct. Mol. Biol.* **2008**, *15*, 558−566.
(7) Hudson, S. A.; Ecroyd, H.; Dehle, F. C.; Musgrave, I. F.; Carver, J. A. *J. Mol. Biol.* **2009**, *392*, 689−700.
(8) Ehrnhoefer, D. E.; Duennwald, M.; Markovic, P.; Wacker, J. L.; Engemann, S.; Roark, M.; Legleiter, J.; Marsh, J. L.; Thompson, L. M.; Lindquist, S.; Muchowski, P. J.; Wanker, E. E. *Hum. Mol. Genet.* **2006**, *15*, 2743−2751.
(9) Bieschke, J.; Russ, J.; Friedrich, R. P.; Ehrnhoefer, D. E.; Wobst, H.; Neugebauer, K.; Wanker, E. E. *Proc. Natl. Acad. Sci. U. S. A.* **2010**, *107*, 7710−7715.
(10) Lorenzen, N.; Nielsen, S. B.; Yoshimura, Y.; Vad, B. S.; Andersen, C. B.; Betzer, C.; Kaspersen, J. D.; Christiansen, G.; Pedersen, J. S.; Jensen, P. H.; Mulder, F. A. A.; Otzen, D. E. *J. Biol. Chem.* **2014**, *289*, 21299−21310.
(11) Yang, J. E.; Rhoo, K. Y.; Lee, S.; Lee, J. T.; Park, J. H.; Bhak, G.; Paik, S. R. *Sci. Rep.* **2017**, *7*, 17945.
(12) Ono, K.; Hasegawa, K.; Naiki, H.; Yamada, M. *J. Neurosci. Res.* **2004**, *75*, 742−750.
(13) Yang, F.; Lim, G. P.; Begum, A. N.; Ubeda, O. J.; Simmons, M. R.; Ambegaokar, S. S.; Chen, P. P.; Kayed, R.; Glabe, C. G.; Frautschy, S. A.; Cole, G. M. *J. Biol. Chem.* **2005**, *280*, 5892−5901.
(14) Thapa, A.; Jett, S. D.; Chi, E. Y. *ACS Chem. Neurosci.* **2016**, *7*, 56−68.
(15) Yoshida, W.; Kobayashi, N.; Sasaki, Y.; Ikebukuro, K.; Sode, K. *Int. J. Mol. Sci.* **2013**, *14*, 2590−2600.
(16) Tsukakoshi, K.; Yoshida, W.; Kobayashi, M.; Kobayashi, N.; Kim, J.; Kaku, T.; Iguchi, T.; Nagasawa, K.; Asano, R.; Ikebukuro, K.; Sode, K. *ACS Chem. Neurosci.* **2018**, *9*, 2898−2903.
(17) Lo Bianco, C.; Shorter, J.; Régulier, E.; Lashuel, H.; Iwatsubo, T.; Lindquist, S.; Aebischer, P. *J. Clin. Invest.* **2008**, *118*, 3087−3097.
(18) Fukui, N.; Araki, K.; Hongo, K.; Mizobata, T.; Kawata, Y. *J. Biol. Chem.* **2016**, *291*, 25217−25226.
(19) Yamamoto, H.; Fukui, N.; Adachi, M.; Saiki, E.; Yamasaki, A.; Matsumura, R.; Kuroyanagi, D.; Hongo, K.; Mizobata, T.; Kawata, Y. *Int. J. Mol. Sci.* **2019**, *21*, 47.
(20) Villmow, M.; Baumann, M.; Malesevic, M.; Sachs, R.; Hause, G.; Fändrich, M.; Balbach, J.; Schiene-Fischer, C. *Biochem. J.* **2016**, *473*, 1355−1368.
(21) Iwasa, H.; Kameda, H.; Fukui, N.; Yoshida, S.; Hongo, K.; Mizobata, T.; Kobayashi, S.; Kawata, Y. *Biochemistry* **2013**, *52*, 9202−9211.
(22) Liu, F.; Zhao, F.; Wang, W.; Sang, J.; Jia, L.; Li, L.; Lu, F. *Food Funct.* **2020**, *11*, 2573−2587.
(23) Yamakawa, M. Y.; Uchino, K.; Watanabe, Y.; Adachi, T.; Nakanishi, M.; Ichino, H.; Hongo, K.; Mizobata, T.; Kobayashi, S.; Nakashima, K.; Kawata, Y. *Nutr. Neurosci.* **2016**, *19*, 32−42.
(24) Vepsäläinen, S.; Koivisto, H.; Pekkarinen, E.; Mäkinen, P.; Dobson, G.; McDougall, G. J.; Stewart, D.; Haapasalo, A.; Karjalainen, R. O.; Tanila, H.; Hiltunen, M. *J. Nutr. Biochem.* **2013**, *24*, 360−370.
(25) Shih, P.-H.; Wu, C.-H.; Yeh, C.-T.; Yen, G.-C. *J. Agric. Food Chem.* **2011**, *59*, 1683−1689.
(26) Yamasaki, H.; Uefuji, H.; Sakihama, Y. *Arch. Biochem. Biophys.* **1996**, *332*, 183−186.
(27) Youdim, K. A.; Martin, A.; Joseph, J. A. *Free Radic. Biol. Med.* **2000**, *29*, 51−60.
(28) De Rosso, V. V.; Morán Vieyra, F. E.; Mercadante, A. Z.; Borsarelli, C. D. *Free Radic. Res.* **2008**, *42*, 885−891.
(29) Meng, F.; Marek, P.; Potter, K. J.; Verchere, C. B.; Raleigh, D. P. *Biochemistry* **2008**, *47*, 6016−6024.
(30) Suzuki, Y.; Brender, J. R.; Hartman, K.; Ramamoorthy, A.; Marsh, E. N. G. *Biochemistry* **2012**, *51*, 8154−8162.
(31) Palhano, F. L.; Lee, J.; Grimster, N. P.; Kelly, J. W. *J. Am. Chem. Soc.* **2013**, *135*, 7503−7510.
(32) Ban, T.; Hoshino, M.; Takahashi, S.; Hamada, D.; Hasegawa, K.; Naiki, H.; Goto, Y. *J. Mol. Biol.* **2004**, *344*, 757−767.
(33) Young, L. J.; Kaminski Schierle, G. S.; Kaminski, C. F. *Phys. Chem. Chem. Phys.* **2017**, *19*, 27987−27996.
(34) Muramatsu, H.; Dicks, J. M.; Tamiya, E.; Karube, I. *Anal. Chem.* **1987**, *59*, 2760−2763.
(35) Liu, Y.; Yu, X.; Zhao, R.; Shangguan, D.-H.; Bo, Z.; Liu, G. *Biosens. Bioelectron.* **2003**, *19*, 9−19.
(36) Ogi, H.; Naga, H.; Fukunishi, Y.; Hirao, M.; Nishiyama, M. *Anal. Chem.* **2009**, *81*, 8068−8073.
(37) Ogi, H.; Motoshisa, K.; Matsumoto, T.; Hatanaka, K.; Hirao, M. *Anal. Chem.* **2006**, *78*, 6903−6909.
(38) Ogi, H.; Motohisa, K.; Hatanaka, K.; Ohmori, T.; Hirao, M.; Nishiyama, M. *Biosens. Bioelectron.* **2007**, *22*, 3238−3242.
(39) Ogi, H.; Fukukshima, M.; Hamada, H.; Noi, K.; Hirao, M.; Yagi, H.; Goto, Y. *Sci. Rep.* **2014**, *4*, 6960.
(40) Hamada, H.; Ogi, H.; Noi, K.; Yagi, H.; Goto, Y.; Hirao, M. *Jpn. J. Appl. Phys.* **2015**, *54*, 07HE01.
(41) Prior, R. L.; Wu, X. *Free Radic. Res.* **2006**, *40*, 1014−1028.
(42) Kalt, W.; Blumberg, J. B.; McDonald, J. E.; Vinqvist-Tymchuk, M. R.; Fillmore, S. A. E.; Graf, B. A.; O'Leary, J. M.; Milbury, P. E. *J. Agric. Food Chem.* **2008**, *56*, 705−712.
(43) Sauerbrey, G. n. *Z. Phys.* **1959**, *155*, 206−222.
(44) Ogi, H.; Fukunishi, Y.; Yanagida, T.; Yagi, H.; Goto, Y.; Fukushima, M.; Uesugi, K.; Hirao, M. *Anal. Chem.* **2011**, *83*, 4982−4988.
(45) Taniguchi, S.; Suzuki, N.; Masuda, M.; Hisanaga, S.-i.; Iwatsubo, T.; Goedert, M.; Hasegawa, M. *J. Biol. Chem.* **2005**, *280*, 7614−7623.
(46) Tang, L.; Zuo, H.; Shu, L. *J. Lumin.* **2014**, *153*, 54−63.
(47) Skemiene, K.; Liobikas, J.; Borutaite, V. *FEBS J.* **2015**, *282*, 963−971.
(48) Parrado-Fernández, C.; Sandebring-Matton, A.; Rodriguez-Rodriguez, P.; Aarsland, D.; Cedazo-Mínguez, A. *Biochim. Biophys. Acta* **2016**, *1862*, 2110−2118.
(49) Mazewski, C.; Kim, M. S.; Gonzalez de Mejia, E. *Sci. Rep.* **2019**, *9*, 11560.
(50) Xiao, J.; Suzuki, M.; Jiang, X.; Chen, X.; Yamamoto, K.; Ren, F.; Xu, M. *J. Agric. Food Chem.* **2008**, *56*, 2350−2356.
(51) Ono, K.; Yoshiike, Y.; Takashima, A.; Hasegawa, K.; Naiki, H.; Yamada, M. *J. Neurochem.* **2003**, *87*, 172−181.
(52) Meng, X.; Munishkina, L. A.; Fink, A. L.; Uversky, V. N. *Biochemistry* **2009**, *48*, 8206−8224.
(53) Meng, X.; Munishkina, L. A.; Fink, A. L.; Uversky, V. N. *J. Parkinsons Dis.* **2010**, *2010*, 650794.
(54) Arita-Morioka, K.-i.; Yamanaka, K.; Mizunoe, Y.; Tanaka, Y.; Ogura, T.; Sugimoto, S. *Sci. Rep.* **2018**, *8*, 8452.
(55) Liu, Y.; Wang, S. H.; Dong, S. Z.; Chang, P.; Jiang, Z. F. *RSC Adv.* **2015**, *5*, 62402−62413.
(56) Ishii, T.; Minoda, K.; Bae, M.-J.; Mori, T.; Uekusa, Y.; Ichikawa, T.; Aihara, Y.; Furuta, T.; Wakimoto, T.; Kan, T.; Nakayama, T. *Mol. Nutr. Food Res.* **2010**, *54*, 816−822.
(57) Zinellu, A.; Sotgia, S.; Scanu, B.; Pisanu, E.; Giordo, R.; Cossu, A.; Posadino, A. M.; Carru, C.; Pintus, G. *J. Chromatogr. A* **2014**, *1367*, 167−171.
(58) Wu, C.; Biancalana, M.; Koide, S.; Shea, J.-E. *J. Mol. Biol.* **2009**, *394*, 627−633.

https://doi.org/10.1021/acs.analchem.1c01720
Anal. Chem. 2021, 93, 11176−11183